Appl Phys B (2011) 104:873–881
DOI 10.1007/s00340-011-4407-5

Applied Physics B
Lasers and Optics

Upconversion excitations in Pr^{3+}-doped BaY_2F_8 crystal

R. Piramidowicz · R. Mahiou · P. Boutinaud · M. Malinowski

Received: 29 November 2010 / Published online: 18 February 2011

Abstract We report the orange-to-blue and infrared-(IR)-to-blue wavelengths upconversion luminescence in Pr^{3+}:BaY_2F_8 crystals. Mechanism of the orange light upconversion into blue $^3P_0$ state emission was confirmed to be energy transfer between two Pr^{3+} ions in the $^1D_2$ state. IR-to-blue upconversion has only been observed under two different color IR pumping. The first resonant step was the $^3H_4 \rightarrow {}^1G_4$ ground state absorption transition, and the second resonant transition was the excited state absorption from the $^1G_4$ to $^1I_6$ and ^3P_J levels. A comparison of the efficiency of the IR-to-blue upconversion in several praseodymium activated host is presented and discussed. A model of the IR pumped upconversion praseodymium blue laser is presented and the population inversion conditions are calculated.

1 Introduction

Praseodymium ion has attracted considerable attention in the last years, particularly for its great potential as multi-wavelength laser activator for various applications. Especially, applications in full-color displays, optical data storage, confocal microscopy, and biomedical instruments have stimulated the development of lasers in the visible spectral range. These kinds of laser devices are frequently based upon Pr^{3+}-doped crystalline or glassy hosts [1, 2]. The low phonon hosts are especially attractive materials because they demonstrate relatively low nonradiative transition rates and can allow normally inactive rare-earth transitions to become optically active. For example, investigations of triply ionized praseodymium-doped $LaCl_3$ have led to the discovery of several new laser transitions in the mid-infrared range between 1.3 and 7.2 μm [3]. Also upconversion processes, which produce population in an excited state which energy exceeds that of the pump photon and often result in emission at shorter wavelengths than that of the pump radiation, are easier to obtain in low phonon systems [2, 4].

Praseodymium activated crystals of $SrAl_{12}O_{19}$ [5], $LiYF_4$ [6], $GdLiF_4$ [7], $LaCl_3$ [8] have been demonstrated to lase in the blue part of the spectrum between transitions from the excited $^3P_0$ state to the ground $^3H_4$ state under direct one photon excitation conditions. This blue emission at about 490 nm can also be excited using the frequency conversion processes due to energy transfer (ET), excited state absorption (ESA) or photon avalanche (PA) [2, 4, 9]. Especially, upconversion processes in Pr^{3+} doped low phonon crystals and ZBLAN glass fibers have been the subject of extensive studies [10, 11].

Orange-to-blue wavelength upconversion due to ET between two Pr^{3+} ions excited to the $^1D_2$ states has been observed in various hosts and is relatively well known [12, 13]. The process of upconversion after IR pumping is less extensively studied despite its importance for blue wavelength lasing under laser diode excitation demonstrated, for example, in Pr^{3+}: ZBLAN fibers [14, 15].

Recently, we have investigated visible Pr^{3+} emission under one color infrared pumping in Pr^{3+} doped $LiNbO_3$, $Be_2La_2O_5$, $YAlO_3$, YAG, GGG and $LiYF_4$ crystals [16–20]. The responsible process was identified as the two step absorption where the first step is non-resonant GSA and the second step is ESA from the lower Stark levels of the $^1G_4$

R. Piramidowicz · M. Malinowski (✉)
Institute of Microelectronics and Optoelectronics PW,
ul. Koszykowa 75, 00-662 Warsaw, Poland
e-mail: m.malinowski@elka.pw.edu.pl
Fax: +48-22-6288740

R. Mahiou · P. Boutinaud
Laboratoire des Matériaux Inorganiques, UMR-6002, Université Blaise Pascal and ENSCCF, 63-177 Aubiere Cedex, France

state to $^1I_6$ and ^3P_J levels of Pr^{3+}. This type of upconversion has been once communicated for Pr^{3+}: BaY_2F_8 (BYF) [21] but, to our knowledge, never reported in detail. Recently Osiac et al. characterized the upconverted $^3P_0$ emission in Pr^{3+}+Yb^{3+}:BYF under the avalanche excitation around 820 and 870 nm [22, 23]. Also, energy level structures for Pr^{3+} in BYF have been reported [23–25].

The aim of this work is twofold: first, to study the upconversion processes in praseodymium doped BYF crystal, and second, to compare and discuss IR-to-visible efficiency in this system with other hosts studied earlier.

2 Experimental

Barium yttrium fluoride BaY_2F_8 (abbreviated BYF) has the monoclinic structure with two molecules per unit cell and space group symmetry $C^3_{2/h}$. The rare-earth ions enter the lattice at yttrium sites having a low C_2 point symmetry. Each rare-earth ion is surrounded by 8 fluoride anions, the shortest separation between the two RE ions is $R_0 = 3.705$ Å. BYF is a biaxial crystal, the main symmetry axis is the crystallographic b-axis which is perpendicular to the a- and c-axes. In BYF, the Pr^{3+} energy levels have non-Kramers character; as a result of the low site symmetry, each of the $^{2S+1}L_J$ manifolds gives rise to a total splitting of $2J + 1$ Stark-level components.

BYF:Pr^{3+} crystal with nominal concentrations of 0.5 at.% was grown using the Czochralski technique at Minsk Polytechnic. The dimensions of the sample were $6 \times 4 \times 3$ mm^3 and it was oriented and cut in the plane of the b- and c-crystallographic axes.

Polarized absorption measurements, in the range from 300 to 1100 nm, were made using Cary 2300 Varian spectrometer equipped with a continuous flow helium cryostat. Fluorescence and excitation spectra were obtained using a Continuum OPO, dye laser or pulsed Ti:sapphire laser, all pumped by a Continuum Surelite II Nd:YAG laser (10 ns pulse length, 10 Hz repetition rate and 180 mJ energy per pulse at 532 nm). The spectra were recorded using Jobin-Yvon or GDM-1000 1 m monochromators with dispersion of 8 Å/mm and detected by EMI 9789 or RCA C31034-02 cooled AsGa photomultipliers. Data acquisition was obtained with a Stanford SR400 single photon counter or PAR 162 boxcar average controlled with a PC. Fluorescence lifetime measurements were made using a LeCroy 9310A 400 MHz oscilloscope and Stanford SR430 multichannel analyzer. Sample cooling was provided by a closed cycle He optical cryostat which allowed the temperature to be varied between 10 and 300 K.

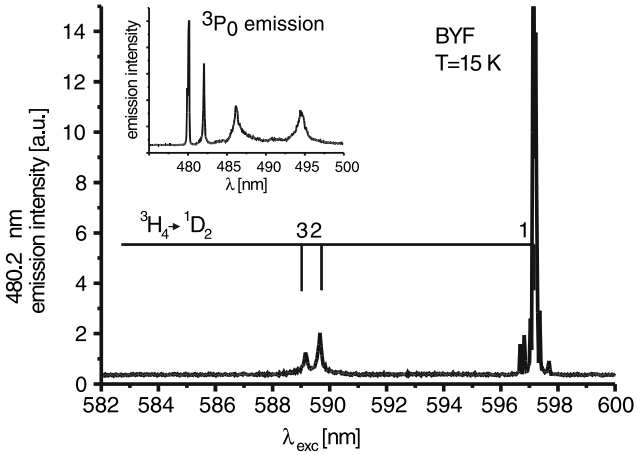

Fig. 1 Excitation spectrum of the emission at 480 nm corresponding to the $^3P_0 \rightarrow {}^3H_4(1)$ transition, the spectrum of which is shown in the *inset*

3 Results

3.1 Orange wavelength excitation

First, the temporal evolution of one-photon, directly excited blue $^3P_0 \rightarrow {}^3H_4$ (480 nm) and red $^1D_2 \rightarrow {}^3H_5$ (713.9 nm) emissions were registered. Both decays were found to be nearly exponential, giving low temperature of 10 K, decay times of 51 and 507 μs for $^3P_0$ and $^1D_2$ emission, respectively.

Blue anti-Stokes luminescence was observed for several wavelengths of excitation lying between 580 and 600 nm. The excitation spectrum of the line located at 480 nm, which corresponds to the $^3P_0 \rightarrow {}^3H_4(1)$ transition, is presented in Fig. 1. The excitation lines at 589.1, 589.6 and 597.1 nm are assigned to the $^3H_4(1) \rightarrow {}^1D_2(1, 2, 3)$ transitions [23, 24]. This is also confirmed by the excitation spectrum of the $^1D_2$ emission at 713.9 nm. Excitation spectra of the anti-Stokes $^3P_0$ and Stokes $^1D_2$ emissions in the vicinity of the lowest Stark component of the $^1D_2$ manifold at 597.1 nm (16746 cm^{-1}) are shown in Fig. 2. As could be seen, this transition exhibits a pronounced additional satellite structure. The decay profiles of the blue anti-Stokes emission after selective excitation of the center of the main line and the satellites are also shown on the right hand side of Fig. 2. The common feature of these decays is that they exhibit a rise time and decay time which is different from that resulting after direct excitation. Excitation at the line center D gives intense $^3P_0$ emission with a rise time of about 18 μs and the decay which is nonexponential with a long time constant of 228 μs. Excitation into the G line ($\Delta E = 15$ cm^{-1}) results in the rise time of 0.5 μs and the decay time of 32 μs, when pumping the C line ($\Delta E = -2$ cm^{-1}), the rise time is 4.5 μs and the decay time is 92 μs. Pumping into the A absorption

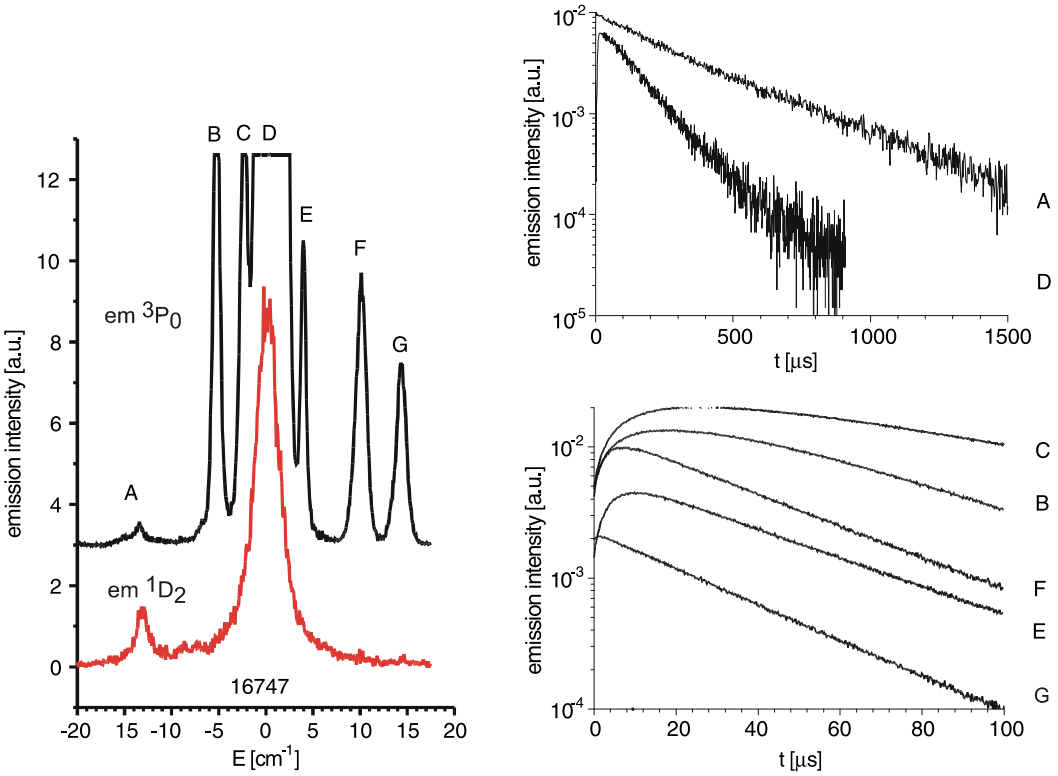

Fig. 2 Excitation spectra of the 480 nm anti-Stokes $^3P_0$ and 713 nm Stokes $^1D_2$ emissions in the vicinity of the lowest Stark component of the $^1D_2$ manifold at 597.1 nm (16746 cm^{-1}). Selectively excited fluorescence decays of the upconverted $^3P_0$ emission, $T = 15$ K

line results in different upconversion dynamics, with no observable rise time and relatively slow decay of 610 μs.

The blue upconverted fluorescence of $^3P_0$ state exhibits well quadratic dependence on orange excitation power.

3.2 Infrared wavelength excitation

In order to optimize excitation conditions, the energy level structure of the $^1G_4$ multiplet in BYF was studied in detail. The polarized excitation spectra of the strong praseodymium-ion fluorescence at around 1:3 μm, which is due to the $^1G_4 \rightarrow {}^3H_5$ transition [25], have been registered and are shown in Fig. 3. It could be seen that relatively wide and strong absorption lines are in the 940 nm band.

First, the sample was illuminated with a pulsed tunable IR laser. However, under this one color IR pumping, we did not observe any visible anti-Stokes emission.

Next, two color excitation experiments were performed when the first laser was fixed at the $^1G_4$ absorption at 940 nm and the second laser was tuned between 750 and 900 nm. In this two-color pumping scheme, the blue anti-Stokes $^3P_0$ emission at 480 nm was observed and registered; results are shown in Fig. 4. The decay profile of the blue emission, resulting from the simultaneous IR excitation at 940 and 830 nm, together with the directly excited $^3P_0$ emission decay profile is shown in the inset of Fig. 4.

The blue upconverted fluorescence of $^3P_0$ state exhibits quadratic dependence on IR pumping power.

4 Discussion

The main features of the orange-to-blue wavelength upconversion, which are the quadratic dependence of the anti-Stokes $^3P_0$ emission and its dynamic showing the short rise time followed by the decay time which is close to the half of its intrinsic decay time, are characteristic for ET upconversion mechanism. It is recognized [12, 13, 18] that the praseodymium ion pair interaction of the type $^1D_2(1) + {}^1D_2(1) \rightarrow {}^1G_4(8) + {}^3P_2(2) + E_{\text{phonon}}$ is responsible for upconversion. In this process, when both ions of a pair are excited to the $^1D_2$ state, a transfer occurs by which one ion loses energy and goes to the lower excited level $^1G_4$, while the second one gains energy and goes to the $^3P_2$ level from which, after rapid non-radiative decay, the $^3P_0$ level is populated. In Pr^{3+}:BYF, the excess energy of 57 cm^{-1} is released.

The time evolution of the $^3P_0$ emission after $^1D_2$ excitation is strongly excitation wavelength dependent. When exciting at the center of the $^3H_4(1) \rightarrow {}^1D_2(1)$ absorption line

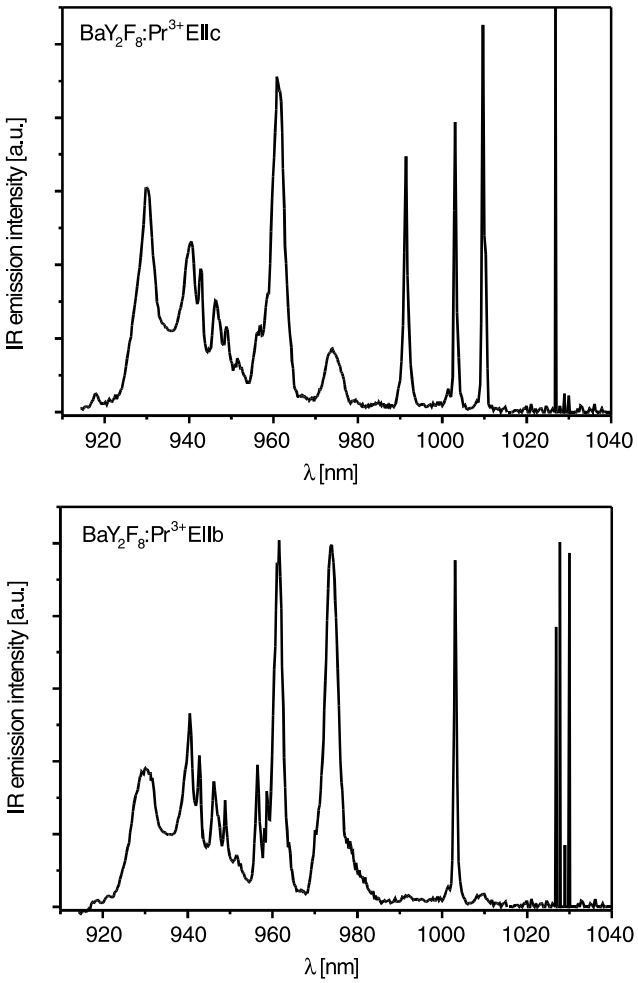

Fig. 3 Polarized excitation spectra of the praseodymium ion fluorescence at 1.3 μm, corresponding to the $^1G_4 \rightarrow {}^3H_5$ transition, $T = 15$ K

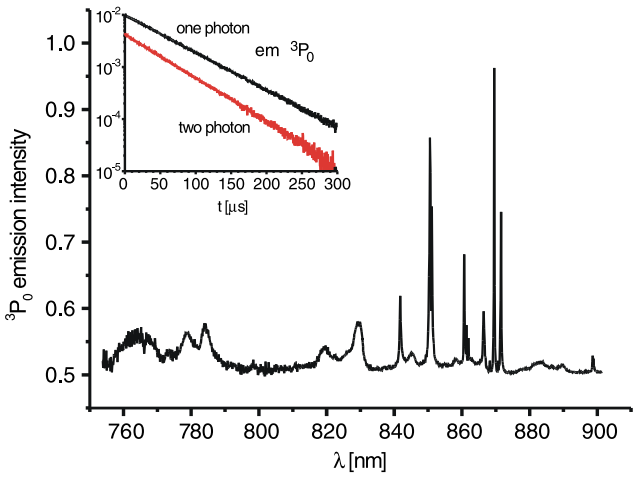

Fig. 4 Two color excitation spectrum of the blue anti-Stokes $^3P_0$ emission at 480 nm, first laser was fixed at the $^1G_4$ absorption at 940 nm when the second laser was tuned between 750 and 900 nm. The *inset* shows dynamics of the Stokes and anti-Stokes $^3P_0$ luminescence, $T = 15$ K

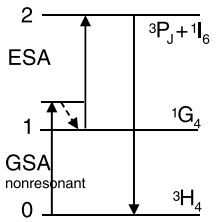

Fig. 5 Generic scheme of the IR-to-blue upconversion in Pr^{3+} ion

at 16747 cm^{-1} the $^3P_0$ decay is nearly exponential with the long time decay approaching the 228 μs value which is close to half of the lifetime of 507 μs. Pumping at B, C, E, F and G satellites results in much faster decays and the rise times, which follows the dependence on the energy difference from the center D line. These observations, which confirm the pair origin interaction, are consistent with the results for other investigated Pr^{3+} systems [12, 13, 18].

By fitting the decay curves with the solution of the population equation for the doubly excited pairs [13, 18], the upconversion energy transfer rates W_{ti} were determined to be $W_{tG} = 1.3 \times 10^6$ s^{-1}, $W_{tF} = 0.34 \times 10^6$ s^{-1}, $W_{tE} = 0.15 \times 10^6$ s^{-1}, $W_{tB} = 0.085 \times 10^6$ s^{-1} and $W_{tC} = 0.047 \times 10^6$ s^{-1}. By fitting the upconverted $^3P_0$ signal resulting from the excitation of the center of absorption line D, the transfer rate $W_{tD} = 0.008 \times 10^6$ s^{-1} has been found, which is in reasonable agreement with the pair upconversion transfer rate measured for Pr^{3+}:YAG [26].

As the transfer rates are a function of ion–ion distances R_i in the approximation of electric dipole–dipole interaction, they are given by $W_t = W_{t0}(\frac{R_i}{R_0})^6$ where W_{t0} and R_0 are the nearest-neighbor transfer rate and distance, respectively. By assuming $W_{tG} = W_{t0}$ and using the calculated transfer rates, the sequence of corresponding inter-ionic distances is calculated to be 3.705, 4.53, 5.13, 5.63 and 6.10 Å, which reproduces well the sequence of Pr–Pr distances in BaY_2F_8 lattice, which are 3.705, 3.822, 4.264, 5.271, 5.649 and 6.148 Å. It is assumed here that two nearest pair lines, 3.705 and 3.822 Å apart, are not spectrally distinguished during our experiments. The origin of line A is not clear, it presents different dynamics and could be related to same irregular or impurity site.

When analyzing the infrared-to-blue upconversion, the first important observation was, in the contrary to various examined earlier hosts [17–20], the absence of the $^3P_0$ emission under one color IR excitation. In all earlier observed praseodymium materials, the process responsible for IR-to-blue upconversion was recognized to be ESA from the $^1G_4$ levels. The general three-level scheme of this ESA is shown in Fig. 5. The intermediate 1 ($^1G_4$) level could be excited directly by the GSA absorption or by the radiative or nonradiative relaxation from the higher lying levels. In the second step, the second photon is absorbed, which brings the ion to the higher lying excited state 2 ($^1I_6 + {}^3P_J$) which decays to the $^3P_0$ level from which light is emitted. It is also important that the intermediate state, which

Table 1 Comparison of the spectroscopic data for various praseodymium activated materials and the calculated GSA and ESA cross-sections

Material		$h\varpi_{max}$ [cm^{-1}]	σ_{GSAel} [10^{-22} cm^2]	ΔE [cm^{-1}]	σ_{GSANR} [10^{-26} cm^2]	σ_{ESA} [10^{-20} cm^2]	N $\Delta E/h\varpi_{max}$	$\tau_2(^3P_0)$ [μs]	$\tau_1(^1G_4)$ [μs]
$Be_2La_2O_5$	BLO	1100	2.8	505	77.6	3.78	0.46	2	~0.2
$LiNbO_3$	LNB	880	3.45	352	83.5	3.92	0.40	0.45	~0.1
$Y_3Al_5O_{12}$	YAG	850	2.75	542	20.3	4.38	0.64	10	0.4
$Gd_3Ga_5O_{12}$	GGG	740	2.55	556	5.99	5.00	0.75	14	0.5
$YAlO_3$	YAP	555	2.23	608	4.20	3.04	1.09	11	0.86
$LiYF_4$	YLF	490	1.76	693	1.14	2.43	1.41	38	17
glass	ZBLAN	450	1.32	~725	0.22	1.76	1.61	47	110
BaY_2F_8	BYF	415	1.51	845	0.17	2.00	2.04	50	38

$h\varpi_{max}$ is the maximum energy of the phonon spectrum

acts as an energy storage reservoir, should exhibit a long lifetime allowing high population of excited ions to be created.

From the energy scheme, it resulted that the single color excitation is in a multiphonon sideband of the $^3H_4 \rightarrow {}^1G_4$ transition. This results in a weak absorption and relatively weak population in the $^1G_4$ state. The energy mismatch ΔE, with respect to the transition from the lowest Stark level in the $^1G_4$ multiplet to the $^3P_0$ level, is 845 cm^{-1} in Pr^{3+}:BYF; for other praseodymium materials studied, the results are shown in Table 1. It must be also noted that to fulfill resonances for the $^1G_4 \rightarrow {}^1I_6$ transitions, ΔE in the first step absorption will be larger by about 400 cm^{-1} [23].

From Table 1, it could be seen that, among the investigated materials, only in BYF this nonresonant process demands participation of more than two phonons, $N = 2.04$, which may explain its weakness and the resulting absence of upconversion. It is evident that higher energy phonon matrix favors the first step praseodymium absorption.

For upconversion modeling, the detailed knowledge of the ground $^3H_4$ state and the excited $^1G_4$ state absorption cross-sections is needed. The excited state cross-sections could be calculated using the Judd–Ofelt approach [27, 28], σ_{ESA} is related to the corresponding line strength S by

$$\sigma_{ESA} = \frac{\lambda}{\Delta\lambda}\frac{8\pi^3 e^2}{3ch(2J+1)}\frac{\chi}{n^2}4\pi\varepsilon_0 S \tag{1}$$

where S is calculated with the use of Ω_i intensity parameters and the reduced matrix $\langle U_i\rangle^2$ elements for transitions from the $^1G_4$ level which are taken from [29]. From the analysis of the $\langle U_i\rangle^2$ values, it is seen that spin allowed $^1G_4 \rightarrow {}^1I_6$ transitions are expected to be much more intense than spin forbidden transitions to the ^3P_J levels.

The ground state nonresonant absorption cross-section σ_{GSANR} is difficult to measure. From the analysis of the absorption and excitation spectra in the 800–950 nm range, the value of σ_{GSANR} could be evaluated to be of the order of 10^{-24} cm^2. The multiphonon side-band absorption efficiency could, however, be calculated using approach of Auzel [30] who showed that the probability for Stokes excitation with respect to an energy gap ΔE to the electronic level is given by

$$\sigma_{GSANR} = \sigma_{GSAel}(0)\exp(-\alpha_s \Delta E) \tag{2}$$

where α_s is related to the multiphonon nonradiative decay parameter α_{NR} by $\alpha_s = \alpha_{NR} + (\hbar\omega_{max})^{-1}2/\overline{N}\ln(N/S_0)$, where $h\omega_{max}$ is the cutoff phonon energy in the host, $N = \Delta E/h\omega_{max}$ is the average order of the multiphonon process and S_0 is the Huang–Rhys electron–phonon coupling parameter at 0 K. Using the electronic absorption cross-sections of the $^3H_4 \rightarrow {}^1G_4$ transition σ_{GSAel} determined from the absorption experiments and energy gap values ΔE [31], the multiphonon assisted absorption cross-sections for several praseodymium activated matrix were calculated and are presented in Table 1.

It could be seen that the excited state absorption cross-section values are about five orders of magnitude higher than those for the nonresonant GSA. For the efficiency of the $^3P_0$ excitation, an important factor is the lifetime of the $^1G_4$ level which is also, via nonradiative transition participation, strongly dependent on the phonon spectrum and varies between the fraction of μs in oxides to several tens of μs in fluorides; see Table 1. So there is a concurrence between two host dependent factors because the higher energy phonon matrix favors the efficiency of the first step absorption.

As could be seen from Table 1, the first step absorption cross-section σ_{GSANR} in the nonresonant case has a very small value. So for practical applications it is necessary to maximize GSA absorption cross-section. This could be obtained, as it has been done in this work, by excitation to the maximum of the $^1G_4$ absorption with the consequence that for resonant ESA a second, shorter wave-

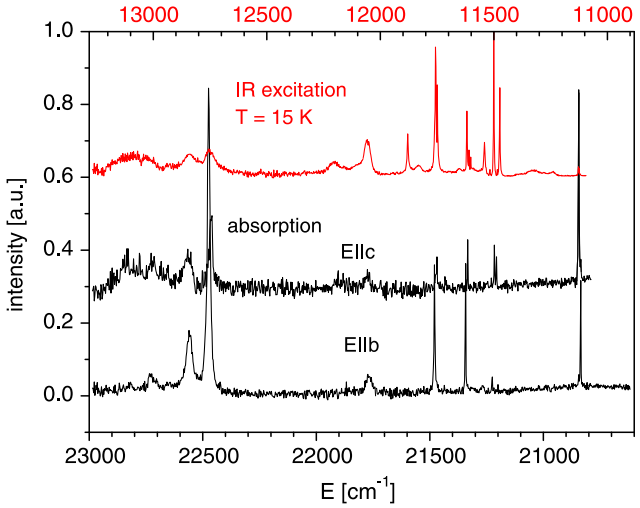

Fig. 6 Comparison of the upconversion excitation spectrum, replotted taking as the origin of energy axis the position of the lowest Stark level in the $^1G_4$ multiplet at 9718 cm^{-1}, with the absorption spectrum

length photon will be needed. Another way is the introduction of Yb^{3+} ions which sensitize Pr^{3+} upconversion process. In this situation, the GSA is dominated by the strong Yb^{3+} $^2F_{7/2} \rightarrow {}^2F_{5/2}$ transition characterized by the σ_{GSAel} of about 1×10^{-20} cm^2 followed by the ET process to the praseodymium $^1G_4$ state. This excitation scheme proved to be efficient, leading to visible $^3P_0$ lasing under one IR color pumping in Pr^{3+}+Yb^{3+} doped YLF, BYF and ZBLAN [2, 32, 33].

Two-color excitation realizes two step resonant pumping scheme where the intermediate 1 ($^1G_4$) level is directly excited by the GSA absorption. The absorption coefficient in the 940 nm band, evaluated from the absorption spectra at 10 K, is $\alpha = 0.01$ cm^{-1}, resulting, with the IR laser excitation energies of the order of 100 μJ focused to the spot of 2×10^{-5} cm^2, in the $^1G_4$ densities of 0.6×10^{20} cm^{-3} corresponding to about 50% excitation. Thus, the excitation spectrum in Fig. 4 is the ESA spectrum corresponding to the $^1G_4 \rightarrow {}^3P_J + {}^1I_6$ transitions. In order to attribute the observed lines, we compared this ESA spectrum, replotted taking as the origin of the energy axis the position of the lowest Stark level in the $^1G_4$ multiplet at 9718 cm^{-1}, with the absorption spectrum. Results of this comparison are shown in Fig. 6.

In the IR excitation spectrum, a group of intense, narrow transitions in the 21500 cm^{-1} range could be observed. From the energy level values reported by Osiac et al. [23], it results that these lines correspond to transitions to the $^3P_1$ and $^1I_6$ Stark levels. As could be expected, spin allowed $^1G_4 \rightarrow {}^1I_6$ transitions are more pronounced, which makes it possible to distinguish between the Stark energy levels of the $^1I_6$ and $^3P_1$ multiplets. The results of this assignment at 10 K are shown in Table 2. These low temperature spectroscopic studies revealed also a Stark level at 9.5 cm^{-1} above the ground (0 cm^{-1}) state in the $^3H_4$ multiplet.

Table 2 Energies of the Stark levels of the $^1I_6$ and $^3P_1$ multiplets in BaY_2F_8 at 15 K

Multiplet	Energy [cm^{-1}]
$^1I_6$	21200, 21218, 21245, 21277, 21315, 21337, 21369, 21395, 21427, 21595, 21890
$^3P_1$	21337, 21479, 21768

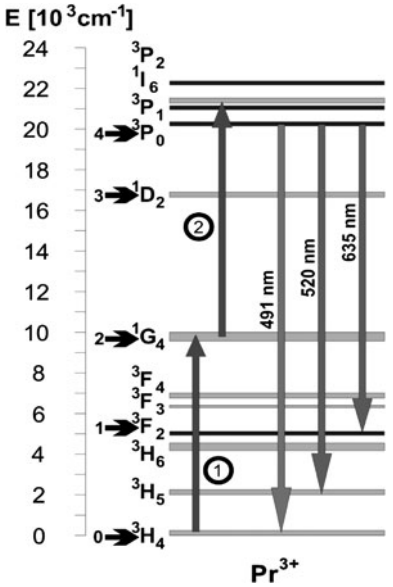

Fig. 7 Simplified energy level scheme of praseodymium ion with two-photon excitation pathway. Energy levels considered in rate equations are arrowed and numbered

5 Modeling

Two-color excitation pumping scheme with two wavelengths λ_1 and λ_2 which are resonant with the ground state absorption transition $Pr(^3H_4) \rightarrow Pr(^1G_4)$ and excited state absorption transition $Pr(^1G_4) \rightarrow Pr(3P_J)$, respectively, is shown in Fig. 7.

In order to analyze operating conditions of the depicted system, a simple rate equation models have been developed [34], which describe approximately the mechanisms leading to optical excitation of the Pr^{3+} $^3P_0$ state. In the case of two-wavelength excitation via ESA, the equations allow easy finding of an analytical solution:

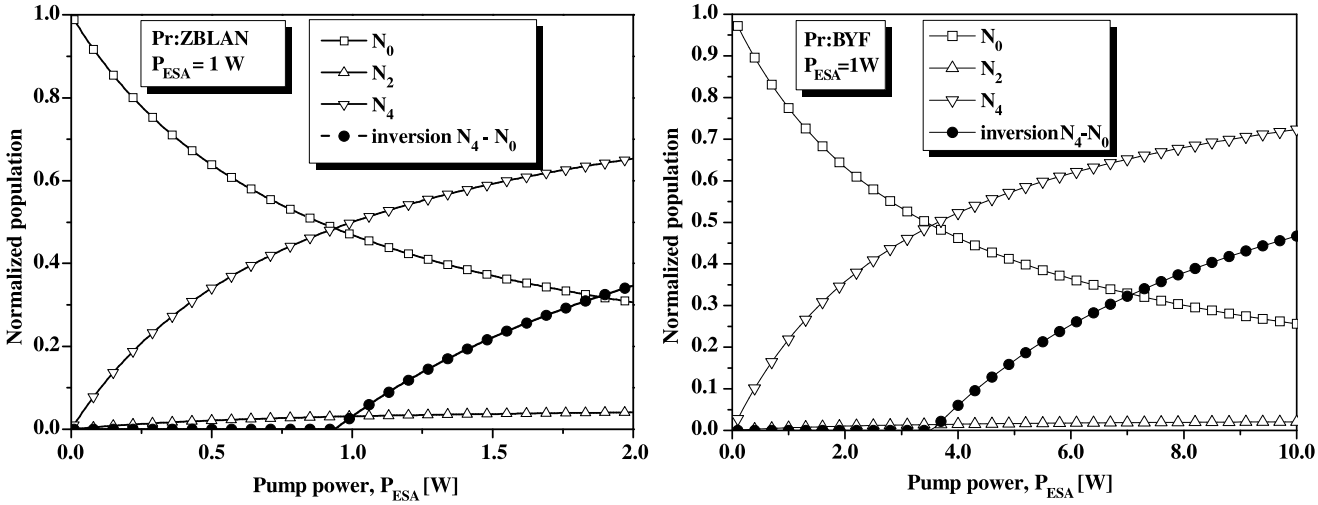

Fig. 8 Pr:ZBLAN and Pr:BYF energy level populations vs. GSA-pump power (P_{GSA})

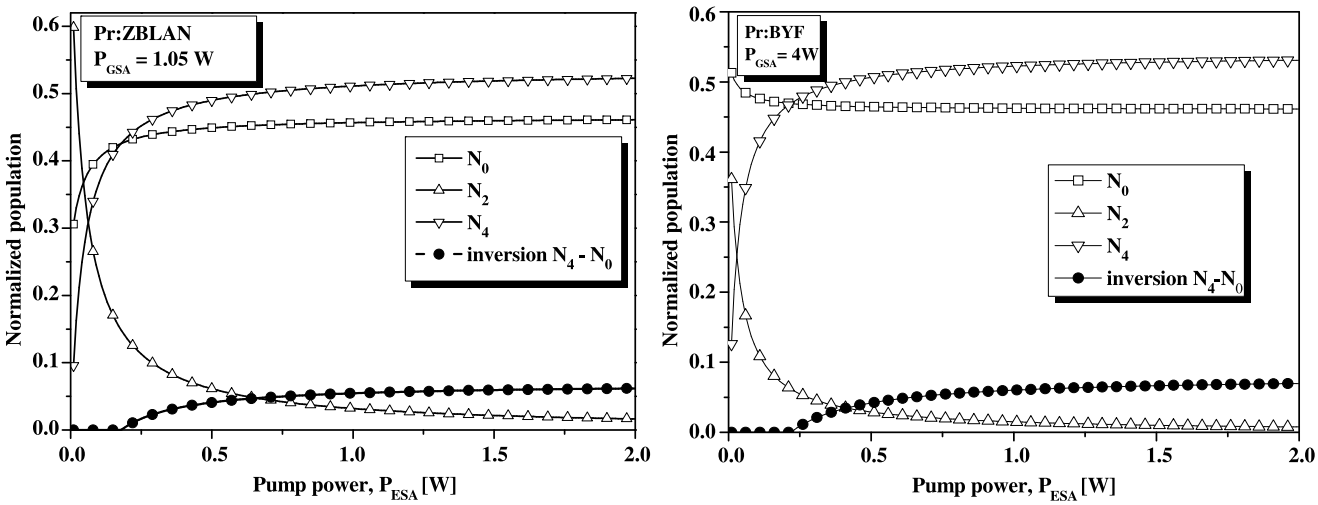

Fig. 9 Pr:ZBLAN and Pr:BYF energy level populations vs. ESA-pump power (P_{ESA})

$$
\begin{aligned}
\frac{\mathrm{d}N_2}{\mathrm{d}t} &= (N_1 - N_2)\cdot W_{\mathrm{ESA12}} - N_2\cdot W_e - N_2\cdot\frac{1}{\tau_2},\\
\frac{\mathrm{d}N_1}{\mathrm{d}t} &= (N_0 - N_1)\cdot W_{\mathrm{GSA01}} - (N_1 - N_2)\cdot W_{\mathrm{ESA12}}\\
&\quad - \mathrm{N}_1\cdot\frac{1}{\tau_1},\\
\frac{\mathrm{d}N_0}{\mathrm{d}t} &= -(N_0 - N_1)\cdot W_{\mathrm{GSA01}} + N_2\cdot W_e + N_2\cdot\frac{1}{\tau_2},\\
N_0 + N_1 + N_2 &= 1,
\end{aligned}
\tag{3}
$$

with

$$
W_{xij} = \frac{I_{xij}\cdot\sigma_{xij}}{h\cdot\nu_{xij}} \tag{4}
$$

as a general formula for transition rate ($x =$ GSA for ground state absorption, $x =$ ESA for excited state absorption and $x = e$ for stimulated emission); i and j indicate the transition levels as shown in Fig. 7, I_{xij} stands for radiation intensity, σ_{xij} is respective absorption/emission cross-section, and ν_{xij} is the transition frequency.

Spectroscopic parameters used in the above equations have been obtained through spectroscopic characterization of the investigated material and are listed in Table 1. The performed analysis applies mainly to an assessment of feasibility of population inversion in the least effective three-level blue laser action scheme (spot size of 2 μm has been assumed). For simplification, the value of W_e was taken as 0, which seems to be a reasonable assumption when only inversion building-up efficiency is analyzed, apart from SE at signal wavelength and resonator specifics.

Figures 8 and 9 show the dependence of the normalized 1 and 2 level populations in Pr:BYF, and for comparison in Pr:ZBLAN also, on pump power. In the first case, ESA-wavelength pump had been fixed at 1 W (which guaran-

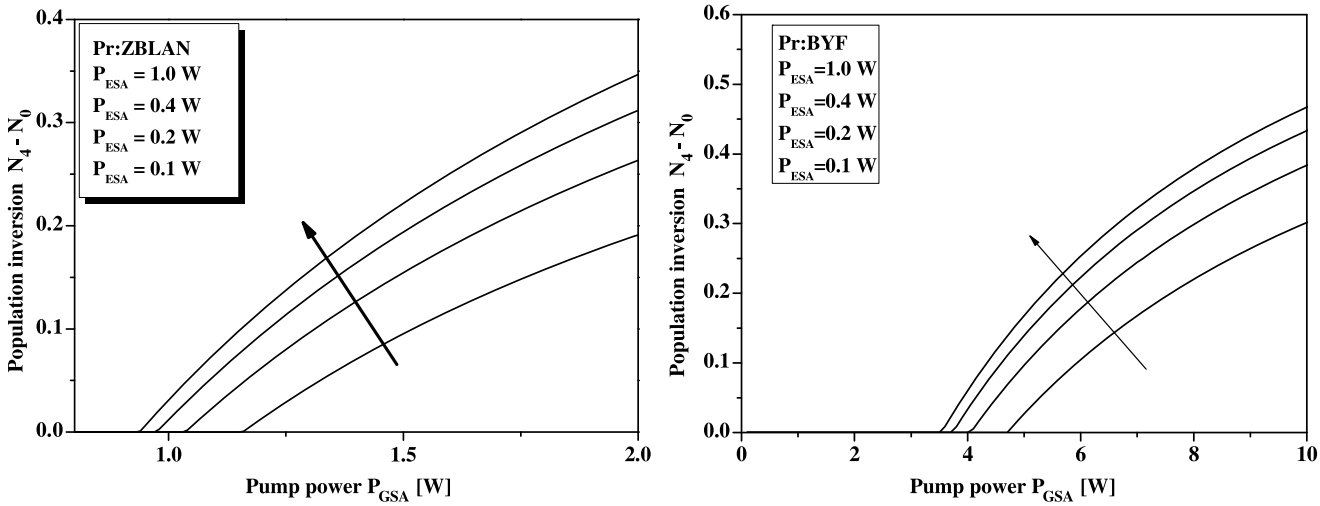

Fig. 10 Population inversion vs. GSA-pump power (P_{GSA})

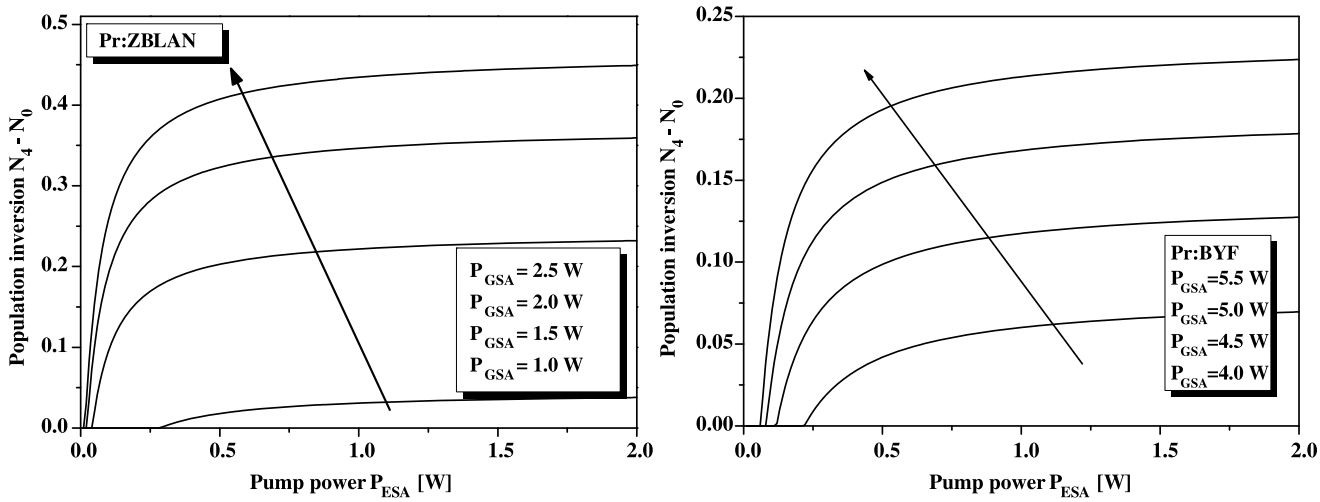

Fig. 11 Population inversion vs. GSA-pump power (P_{ESA})

tees effective pumping via ESA) and population inversion dependence on GSA resonant pump was investigated. Non-negative values of inversion begin to appear when the GSA pump level reaches circa 4 W (in the case of Pr:BYF) and circa 1 W (in the case of Pr:ZBLAN). In both cases, the inversion increases rapidly with further increment of pump power. The difference between required power levels between Pr:BYF and Pr:ZBLAN results mainly from significant difference in the GSA cross-section values (see Table 1) as well as from differences in fluorescence lifetimes of the intermediate $^1G_4$ level.

Fixing the GSA pump power at nearly threshold values of 1 W and 4 W in the case of Pr:ZBLAN and Pr:BYF, respectively, and changing the ESA pump power reveals a threshold values of slightly over 200 mW for obtaining population inversion in both investigated materials and only a moderate dependence on the ESA pump power level (Fig. 9). This difference is explained by a large difference in GSA and ESA absorption cross-section values with this later being two orders of magnitude higher.

This is further examined by analyzing data in Fig. 10, where it can be seen that the ESA-pump power changes of an order of magnitude are not followed by similarly significant changes of population inversion. The data presented in Fig. 11 confirms, on the other hand, that increasing GSA-pump power results in a considerable increase of the upper laser level population over the ground state.

6 Summary

Our studies indicated that in the BaY_2F_8:Pr^{3+} crystal sequential two-photon absorption is responsible for infrared-to-blue wavelength upconversion excitation. We demon-

strated that in BYF:Pr^{3+} IR-to-blue upconversion could only be observed under two wavelengths pumping. This situation is related to the weakness of the nonresonant processes resulting from the low phonon energies in BYF, forbidding efficient excitation with single energy photons. Upconversion excitation with orange light was studied and confirmed to result from the energy transfer process. Finally, conditions for the IR pumped blue upconversion praseodymium lasing are presented and discussed for BaY_2F_8 and ZBLAN matrices.

Recent reports [35–37] demonstrated efficient, room temperature visible lasing in several Pr-activated fluoride crystals under direct GaN diode laser pumping. It seems that further development of GaN-based semiconductor lasers emitting at wavelengths between 350 and 450 nm will allow to more efficiently exploit the potential of Pr^{3+}-doped solid-state lasers.

Acknowledgement M. Malinowski acknowledges Université Blaise Pascal in Clermont Ferrand for supporting his stay as a visiting professor in the Laboratoire des Matériaux Inorganiques.

References

1. A.A. Kaminskii, Phys. Status Solidi A **200**, 215 (2003)
2. H. Scheife, G. Huber, E. Heumann, S. Bär, E. Osiac, Opt. Mater. **26**, 365 (2004)
3. S.R. Bowman, L.B. Shaw, B.J. Feldman, J. Ganem, IEEE J. Quantum Electron. **32**, 646 (1996)
4. J.F. Suyer, A. Aebischer, D. Biner, P. Gerner, J. Grimm, S. Heer, K.W. Krämer, C. Reinhard, H.U. Gudel, Opt. Mater. **27**, 1111 (2005)
5. L.D. Merkle, B. Zandi, Y. Guyot, H.R. Verdun, B. McIntosh, B.H.T. Chai, J.B. Gruber, M.D. Seltzer, C.A. Morrison, R. Moncorge, in *OSA Proc.*, ed. by T.Y. Fan, B.H.T. Chai. Advanced Solid-State Lasers, vol. 20 (1994)
6. L. Esterowitz, R. Allen, M. Krueger, F. Bartoli, L.S. Goldber, H.P. Jenssen, A. Linz, V.O. Nicolai, J. Appl. Phys. **48**, 650 (1977)
7. T. Danger, T. Sandrock, E. Heumann, G. Huber, B. Chai, Appl. Phys. B **57**, 239 (1993)
8. K.R. German, A. Kiel, H. Guggenheim, Appl. Phys. Lett. **22**, 87 (1973)
9. F. Auzel, Chem. Rev. **104**, 139 (2004)
10. R. Balda, J. Fernandez, A. Mendioroz, M. Voda, M. Al-Saleh, Opt. Mater. **24**, 91 (2003)
11. A. Remillieux, B. Jacquier, C. Linares, C. Lesergent, S. Artigaud, D. Bayard, L. Hamon, J.L. Beylat, J. Phys. D, Appl. Phys. **29**, 963 (1996)
12. D.J. Zalucha, J.C. Wright, F.K. Fong, J. Chem. Phys. **59**, 997 (1973)
13. R. Buisson, J.C. Vial, J. Phys. Lett. **42**, L-115 (1981)
14. A.C. Tropper, J.N. Carter, R.D.T. Lauder, D.C. Hanna, S.T. Davey, D. Szebesta, J. Opt. Soc. Am. B **11**, 886 (1994)
15. R.G. Smart, D.C. Hanna, A.C. Tropper, S.T. Davey, S.F. Carter, D. Szebesta, Electron. Lett. **27**, 1307 (1991)
16. R. Piramidowicz, I. Pracka, W. Woliński, M. Malinowski, J. Phys., Condens. Matter **12**, 709 (2000)
17. R. Piramidowicz, M. Kowalska, M. Malinowski, J. Alloys Compd. **300–302**, 430 (2000)
18. M. Malinowski, C. Garapon, M.F. Joubert, B. Jacquier, J. Phys., Condens. Matter **7**, 199 (1995)
19. M. Malinowski, M.F. Joubert, B. Jacquier, Phys. Rev. B **50**, 12367 (1994)
20. M. Malinowski, R. Piramidowicz, J. Sarnecki, W. Woliński, J. Phys., Condens. Matter **10**, 1 (1998)
21. C. Garapon, M.-F. Joubert, B. Jacquier, A.A. Kaminskii, M.D. Faucher, International Conf. of Elements ICFE3, 14–18 September 1997, Paris, Abstract Book P2-69
22. E. Osiac, E. Heumann, G. Huber, S. Kück, E. Sani, A. Toncelli, M. Tonelli, Appl. Phys. Lett. **82**, 3832 (2003)
23. E. Osiac, S. Kück, E. Heumann, G. Huber, E. Sani, A. Toncelli, M. Tonelli, Opt. Mater. **24**, 537 (2003)
24. B. Di Bartolo, B.E. Bowlby, J. Lumin. **102–103**, 481 (2003)
25. C. Garapon, M. Malinowski, M.-F. Joubert, A.A. Kaminskii, B. Jacquier, J. Phys. **4**, 349 (1994)
26. M. Malinowski, P. Szczepański, W. Woliński, R. Wolski, Z. Frukacz, J. Phys., Condens. Matter **5**, 6469 (1993)
27. B.R. Judd, Phys. Rev. **127**, 750 (1962)
28. G.S. Ofelt, J. Chem. Phys. **37**, 511 (1962)
29. A. Kaminskii, *Crystalline Lasers* (CRC Press, Boca Raton, 1996)
30. F. Auzel, Phys. Rev. B **13**, 2809 (1976)
31. R. Piramidowicz, Ph.D. Thesis, Warsaw University of Technology (2000)
32. T. Sandrock, E. Heumann, in *OSA Trends in Optics and Photonics on Advanced Solid-State Lasers*, vol. 1, ed. by S.A. Payne, C.R. Pollock (Optical Society of America, Washington DC, 1996), pp. 550–553
33. D.M. Baney, G. Rankin, K.W. Chang, Appl. Phys. Lett. **69**, 1662 (1996)
34. M. Klimczak, P. Witoński, M. Malinowski, R. Piramidowicz, Proc. SPIE **6599**, 65990J-1 (2007)
35. A. Richter, E. Heumann, G. Huber, V. Ostroumov, W. Seelert, Opt. Express **15**, 5172 (2007)
36. A. Richter, N. Pavel, E. Heumann, G. Huber, D. Parisi, A. Toncelli, M. Tonelli, A. Diening, W. Seelert, Opt. Express **14**, 3282 (2006)
37. K. Hashimoto, F. Kannari, Opt. Lett. **32**, 2493 (2007)